

Topological Valley Transport of Gapped Dirac Magnons in Bilayer Ferromagnetic Insulators

Xuechao Zhai^{1,2} and Yaroslav M. Blanter²

¹*New Energy Technology Engineering Laboratory of Jiangsu Province & School of Science,*

Nanjing University of Posts and Telecommunications (NJUPT), Nanjing 210023, China

²*Kavli Institute of NanoScience, Delft University of Technology, 2628 CJ Delft, The Netherlands*

Bilayer Heisenberg ferromagnetic insulators hold degenerate terahertz Dirac magnon modes associated with two opposite valleys of the hexagonal Brillouin zone. We show that this energy degeneracy can be removed by breaking of the inversion symmetry (\mathcal{I}), leading to a topological magnon valley current. We show furthermore that this current leads to valley Seebeck effect for magnons and is thereby detectable. We perform calculations in the specific example of bilayer CrBr_3 , where \mathcal{I} can be broken by electrostatic doping.

Introduction—Recent discoveries of atomic-thick ferromagnetic (FM) insulators [1, 2] represent a landmark for 2D fundamental and applied physics. Stable long-range 2D FM order strongly relies on the presence of magnetic anisotropy [3–5]. In these materials Magnons, elementary excitations of magnetic structure, usually have spectra with Dirac points. In particular, magnons in two of the most popular 2D FM insulators have been studied experimentally in more detail: Dirac properties protected by inversion symmetry (\mathcal{I}) and time reversal symmetry (\mathcal{T}) in monolayer CrBr_3 [6] and topological gaps induced by \mathcal{T} breaking in monolayer CrI_3 [7].

The graphene-like spectrum of 2D magnons is characterized by the appearance of two valleys — K and K' — of the hexagonal Brillouin zone. The valley index can serve as a quantum number [8–12], and it has been already demonstrated in electron systems [13, 14], and more recently also in 2D photonic [15] and phononic [16] crystals that it can form a basis for quantum information transfer. However, it is very difficult to use the valley degree of freedom for 2D magnons. On one hand, the magnons near K (K') have large momentum and no charge, and thus the usual magnon manipulation methods such as FM resonance [17] or electric, magnetic, or optical methods [13–16] can not easily detect the two valleys, not even speaking about their difference. On the other hand, the concept of Fermi energy is absent for bosonic magnons, and thus one can only thermally excite the (THz) valley magnons [18] simultaneously with other low-frequency modes.

Instead, in order to utilize the valley degree of freedom in 2D magnets, we turn to the concept of topology [19–24]. It is attractive since the topological magnon transport is insensitive to sample defects. The topological current is in principle dictated by the crystal symmetry [20–22], which is difficult to change in 3D systems. The momentum-dependent topological magnon current, odd under \mathcal{T} but even under \mathcal{I} [24–26], is strictly zero in pristine magnon systems respecting both \mathcal{I} and \mathcal{T} — typical FM Heisenberg systems [6, 25]. However, if \mathcal{I} is broken for magnons in FM insulators, \mathcal{T} requires the Hall current to have the opposite values in two valleys, resulting in a magnon valley Hall current, in analogy with electron systems [26–28]. The \mathcal{I} breaking can not be induced by the external electric field, since the localized moments do not change with the electric potential [29], however, it can be induced by layer-dependent electrostatic doping [30] in bilayer magnets.

In this Letter, we explore the topological valley transport of magnons under \mathcal{I} breaking in bilayer Heisenberg FM insulators. We propose that the pure magnon valley current can be detected via the inverse valley Hall effect, and discuss a novel concept of valley Seebeck effect for 2D magnets. We perform calculations for the specific example of bilayer CrBr_3 [31, 32], where \mathcal{I} of magnons (~ 1.8 THz near two valleys) can be broken by electrostatic doping. The results show how the valley degree of freedom can be manipulated in 2D magnets and opens the way of using it for information transfer — THz magnon valleytronics.

Hamiltonian—We consider a bilayer collinear FM insulator on a usual AB-stacked honeycomb lattice with the magnetic anisotropy perpendicular to the hexagon plane, i.e. spins on $\mu = \text{A}\alpha, \text{B}\alpha$ sublattices in the ground state satisfy $\mathbf{S}_{\text{A}\alpha} = \mathbf{S}_{\text{B}\alpha} = S\hat{z}$, where $\alpha = \pm$ indicates the top (bottom) layer, see Fig. 1(a). A general Heisenberg Hamiltonian [3–7] with breaking of \mathcal{I} reads

$$\hat{\mathcal{H}} = - \sum_{\langle i,j \rangle} J_{ij} \mathbf{S}_i \cdot \mathbf{S}_j - \lambda \sum_{\langle i,j \rangle} S_i^z S_j^z + \sum_i \alpha U \hat{z} \cdot \mathbf{S}_i. \quad (1)$$

The first term represents the magnetic exchange interaction with $J_{ij} = J (J_z) > 0$ for intralayer (interlayer) nearest-neighbour magnetic moments. The second term indicates the anisotropic FM exchange with $\lambda > 0$ [4]. The last term H_U indicates \mathcal{I} breaking [discussed in Eq. (11)]. By applied low magnetic field, the FM ground state can be stabilized. The essential physics will not be altered when the second- or third-nearest neighbor exchange interactions are included.

Neglecting the magnon-magnon interactions in Eq. (1), the Holstein-Primakoff (HP) transformation [6] reads $S_{i\mu}^+ \equiv S_{i\mu}^x + iS_{i\mu}^y \simeq \sqrt{2S} c_{i\mu}$, $S_{i\mu}^- \equiv S_{i\mu}^x - iS_{i\mu}^y \simeq \sqrt{2S} c_{i\mu}^\dagger$, $S_{i\mu}^z = S - c_{i\mu}^\dagger c_{i\mu}$. In the A+, B+, A-, B- basis, the Bloch Hamiltonian after HP transformation is expressed as

$$H_{\mathbf{k}} = S \begin{pmatrix} J_z + \gamma + U & -Jf_{\mathbf{k}} & 0 & -J_z \\ -Jf_{\mathbf{k}}^* & \gamma + U & 0 & 0 \\ 0 & 0 & \gamma - U & -Jf_{\mathbf{k}} \\ -J_z & 0 & -Jf_{\mathbf{k}}^* & J_z + \gamma - U \end{pmatrix}, \quad (2)$$

where $f_{\mathbf{k}} = \exp(-ik_y a/2) [2 \cos(\sqrt{3}k_x a/2) + \exp(i3k_y a/2)]$ (a is the hexagon side length) and $\gamma = 3(J + \lambda)$.

We now introduce the Pauli matrices in the sublattice ($\hat{\sigma}$) and layer (τ) spaces, considering $\text{A}\alpha$ and the top layer ($\text{B}\alpha$ and

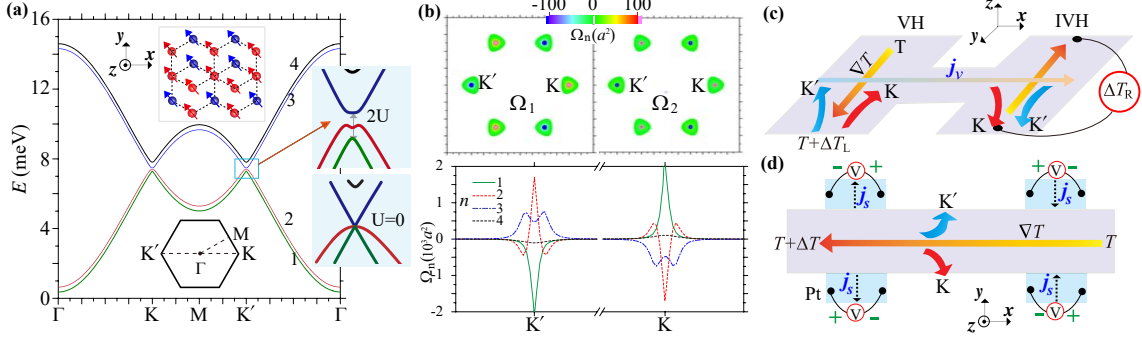


FIG. 1: (a) Magnon spectrum of bilayer CrBr₃ with $J = 1.55$ meV, $J_z = 0.2$ meV, $S = 3/2$, $\lambda = 0.05J$, $a = 3.72$ Å, $d_z = 6.11$ Å [6, 32–34], assuming $U = 0.1$ meV. The top (bottom) inset sketches the structure in real (reciprocal) space. The right inset enlarges the gapped Dirac bands near 7.5 meV $\simeq 1.8$ THz (The case $U = 0$ is plotted for comparison). (b) Berry curvature corresponding to (a). (c) A Hall bar to thermally detect a net pure valley Hall (VH) current \mathbf{j}_v via the inverse VH (IVH) effect. (d) A device of valley Seebeck effect for magnons. Inverse spin Hall (ISH) effect [35, 36] occurs in Pt metallic contact (optionally), where \mathbf{j}_s is the spin current.

the bottom layer) as an up (down) pseudospin, respectively. The index $\xi = \pm$ denotes two valleys K and K' at $(k_x, k_y) = [4\pi/(3\sqrt{3}a)](\pm 1, 0)$. Expanding Eq. (2) near K and K' , we obtain the effective Hamiltonian as

$$H_{\mathbf{q}} = \begin{pmatrix} H_{\mathbf{q}}^K & 0 \\ 0 & H_{\mathbf{q}}^{K'} \end{pmatrix}, \quad H_{\mathbf{q}}^{\xi} = \tau_0 h_{\mathbf{q}}^{\xi} + U_{\gamma} \tau_0 \sigma_0 + J_z S \Gamma, \quad (3)$$

where $\mathbf{q} \equiv \mathbf{k} - \mathbf{K}$ (K'), $U_{\gamma} \equiv (\gamma + \alpha U)S$, $h_{\mathbf{q}}^{\xi} = \hbar v(\xi q_x \sigma_x + q_y \sigma_y)$ (Dirac form [6]) with $v = (3a/2)JS$, and $\Gamma = (\tau_0 \sigma_0 + \tau_z \sigma_z)/2 - \sum_{i=\pm} \tau_i \sigma_i/4$ with $\tau_{\pm} = \tau_x \pm i\tau_y$, $\sigma_{\pm} = \sigma_x \pm i\sigma_y$. Here, τ_0 (σ_0) is the identity matrix of the layer (valley) pseudospin.

The time-reversal operator that interchanges two valleys for magnons in Eq. (3) is found as

$$\hat{\mathcal{T}} = \begin{pmatrix} 0 & \tau_z \sigma_z \\ \tau_z \sigma_z & 0 \end{pmatrix} C = \hat{\mathcal{T}}^{-1}, \quad (4)$$

where C is the operator of complex conjugation. The relation $\hat{\mathcal{T}} \mathcal{H}_{\mathbf{q}} \hat{\mathcal{T}}^{-1} = \mathcal{H}_{\mathbf{q}}$ confirms the time-reversal invariance of the system, leading to the energetically degeneracy of two valleys.

For convenience, we set $\hbar = 1$, $v = 1$ below. For $U = 0$, the eigenvalues of Eq. (3) read $E_n^0 = \gamma S + \varepsilon_n^0$, where $n = 1$ to 4 indexes the subband. Two magnon modes in each valley are massless (Dirac) modes [Fig. 1(a)], $\varepsilon_{1,3}^0 = \mp \mathbf{q}$, and the other two modes have a gap, $\varepsilon_{2,4}^0 = J_z S \mp [q^2 + (J_z S)^2]^{1/2}$. Therefore, a triple degeneracy [25] exists at K (K') point ($q = 0$). For $U \neq 0$, the eigenvalues are $E_n = \gamma S + \varepsilon_n$, \mathcal{I} is broken, the Dirac magnon subbands are gapped [Fig. 1(a)], and the triplet degeneracy in each valley is lifted although the two valleys are energetically degenerate. In contrast, there is no counterpart of this model in 2D electron systems [10–14, 38].

By using perturbation theory (Supplemental Material (SM) [39]) under $U/J_z \ll 1$, we can find the eigenvalues ε_n as

$$\varepsilon_1 \simeq \frac{\Delta_{-}}{2} - \sqrt{2q^2 \cos^2 \frac{\varphi}{2} + \frac{\Delta_{+}^2}{4}}, \quad \varepsilon_4 \simeq \varepsilon_4^0 + \frac{U^2 S}{2J_z} (2 - \cos \theta), \quad (5)$$

where $\Delta_{\pm} = [J_z - (J_z^2 + U^2)^{1/2} \pm U]S$, $\cos \varphi = U/(J_z^2 + U^2)^{1/2}$, $\cos \theta = J_z/(q^2 + J_z^2)^{1/2}$. Here, $\varepsilon_{2,3}(q)$ are not presented due

to their complexity (SM [39]). Specifically, the energies at K (K') read

$$\varepsilon_{1,3}^0 = \mp US, \quad \varepsilon_{2,4}^0 = \left(J_z \mp \sqrt{J_z^2 + U^2} \right) S, \quad (6)$$

agreeing with the numerical result in Fig. 1(a).

Generation of topological valley current.—We consider a rectangular sample with width W and length L . By applying energy-flux quantum theory [40–42] to noninteracting magnons, we obtain the average energy current density as

$$J_{\varepsilon} = \frac{1}{2V} \sum_{\mathbf{k}} u_{mk}^{\dagger} \left(\frac{\partial \mathcal{H}_{\mathbf{k}}}{\partial \mathbf{k}} \right)_{mn} u_{nk}, \quad (7)$$

where $V = WLd_z$ (d_z is the thickness) is the sample volume, and u_{nk} is the Bloch wave function for the n -th subband. Using the Kubo formula acting on J_{ε} [40], the thermal Hall conductivity of magnons can be derived as $\kappa_{xy} = -(k_B^2 T / \hbar V) \sum_{nk} C_{nk} \Omega_{nk}$, where the sum is all over the first Brillouin zone, $C_{nk} = (1 + f_B)[\ln(1 + 1/f_B)]^2 - (\ln f_B)^2 - 2\text{Li}_2(-f_B)$, with $f_B = [\exp(\varepsilon_{nk}/k_B T) - 1]^{-1}$ denoting the Bose-Einstein distribution and Li_2 being the dilogarithm function. The Berry curvature is determined by [26] $\Omega_{nk} = \nabla_{\mathbf{k}} \times \langle u_{nk} | i \nabla_{\mathbf{k}} | u_{nk} \rangle$.

Because the system has \mathcal{T} , the magnons near K and K' can feel the opposite orbit pseudomagnetic field reflected in $\Omega_{nq}^K = -\Omega_{n,-q}^{K'}$, as shown in Fig. 1(b). Our detailed calculations [39] reveal the local conservation law of the Berry curvature [26] $\sum_{n=1}^4 \Omega_{nk} = 0$. We have $\kappa_{xy} = 0$ because the contributions from K and K' cancel each other, however, a pure valley current of magnons is generated. To distinguish the difference between K and K' , it is necessary to define a magnon valley Hall conductivity as $\kappa_{xy}^V \equiv \kappa_{xy}^K - \kappa_{xy}^{K'}$. It has the form

$$\kappa_{xy}^V = -\frac{k_B^2 T}{\hbar V} \sum_{nq} C_{nq} (\Omega_{nq}^K - \Omega_{nq}^{K'}), \quad (8)$$

where the summation over q around valley K (K') runs over

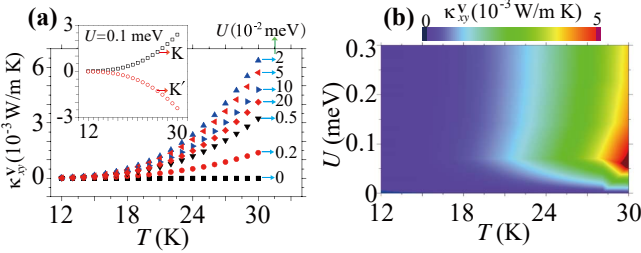


FIG. 2: Valley Hall conductivity (a) as a function of temperature under the influence of U and (b) in the (U, T) plane. The other parameters are taken from CrBr_3 (caption in Fig. 1).

the half of the first Brillouin zone. As we concern in Eq. (3), the pure valley transport occurs due to $\Omega_{nq}^K = -\Omega_{nq}^{K'}$.

Detection.—The signal of topological valley transport κ_{xy}^v can be detected via the inverse magnon valley Hall effect [Fig. 1(c)]. For thermal magnon transport, the directly observable qualities are thermal flux density j_e and temperature difference [40], *e.g.*, ΔT_L and ΔT_R in Fig. 1(c). From the well-known Onsager relation [36], we define a nonlocal thermal resistivity as $\rho_{NL} \equiv \Delta T_R / j_e$. By using the appropriate boundary conditions (SM [39]), we self-consistently derive ρ_{NL} as

$$\rho_{NL} \approx \frac{W}{2\ell_v} \frac{(\kappa_{xy}^v)^2}{(\kappa_{xx})^3} \exp\left(-\frac{L}{\ell_v}\right), \quad (9)$$

where $\kappa_{xx} = j_e / \Delta T_L$ is the local thermal conductivity. Note that Eq. (9) recovers the formula known for spin or valley Hall systems for electrons [20, 43].

An alternative method to detect κ_{xy}^v is by using heat-to-charge conversion [36]. We propose a concept of valley Seebeck effect, as sketched in Fig. 1(d), where Pt contacts (optionally) are added to the sample, and magnons from K , K' accumulate at the opposite sides. Consequently, spin current j_s can be induced in Pt due to s-d interaction (SM [39]) at the FM insulator/Pt metal interface [35–37]. The inverse spin Hall (ISH) electric field in Pt is determined by

$$\mathbf{E}_{ISH} = (\rho \theta_{SH}) \mathbf{j}_s \times \mathbf{s}, \quad (10)$$

where ρ and θ_{SH} indicate the electric resistance and spin Hall angle of Pt, \mathbf{s} is an out-of-plane spin polarization vector. The ISH voltage is in principle determined by [39] $V_{ISH} \propto j_s \propto \Delta T \sinh(x/\lambda_m)$, where $x = 0$ is at the center of the CrBr_3 sample and λ_m is the magnon relaxation length. Because the temperature difference between electrons in Pt and magnons in FM insulator changes sign if the Pt contact is moved from left to right in Fig. 1(d), j_s and the ISH voltage change signs correspondingly [35, 39].

Materials Realization.—Our proposal for topological valley Hall effect of magnons can be experimentally detected in a number of 2D FM insulators. One possibility is bilayer CrBr_3 , which has an electronic band gap about 1.4 eV [44, 45] and $S = 3/2$ for each Cr^{3+} ion [6]. According to experimental results [6, 32, 44], the Hamiltonian (1) without H_U indeed cap-

tures the intrinsic magnon physic of this material, and quantum fluctuations are not as important as that in spin 1/2 systems [24]. In addition, corrections from the single-ion magnetic anisotropy term $H_{\mathcal{A}} = \mathcal{A} \sum_{\langle i,j \rangle} (S_i^z)^2$ shift up the magnon bands by a small energy $2\mathcal{A}$ below 0.1 meV [46]. This effect is not relevant for topological transport dominated by high-energy THz magnons near two valleys.

By applying the electrostatic doping technique [47] to bilayer CrBr_3 , the localized moments in each layer can be continually tuned (more than 20% electron or hole doping was achieved in CrI_3 [30]). For a typical doping case, the two monolayers are doped equally with opposite charges, and the localized moments in the FM ground state can be described as $S_{i,\alpha} = (S - \alpha\Delta S)\hat{z}$. One advantage of this doping is that the variation of parameters J_{\perp} , λ in Eq. (1) can be safely ignored [30]. The \mathcal{I} breaking term H_U has the specific form

$$H_U = \sum_i \alpha U S_i^z \quad \text{with} \quad U = \Delta S. \quad (11)$$

The doping also creates interlayer electric field. However, we expect that it has a minor contribution to ΔS [29] because the two insulating layers are weakly coupled.

Figure 2 shows the results of the calculation of κ_{xy}^v for bilayer CrBr_3 for different U and T . They indicate that κ_{xy}^v is lower than 0.1 mW/m K below 12 K because the Berry curvature for the dominant low-energy magnons away from two valleys is nearly zero [Fig. 1(b)]. Near $T = 30$ K (Curie temperature $T_C = 34$ K [32]), κ_{xy}^v can exceed 6 mW/m K, which is about one order of magnitude greater than the Hall signal reported in 3D FM insulators [42] demonstrating the advantage of Dirac magnons here. We assume a typical value of $\kappa_{xy}/\kappa_{xx} \sim 5 \times 10^{-3}$ (see SM [39], where κ_{xx} contributed from electrons, phonons and magnons are discussed), which agrees with the latest experimental detection in other 2D magnets [48, 49]. By fixing $L = 4W = 2\ell_v$ ($\ell_v \sim 1.0 \mu\text{m}$ is expected from valleytronic experiments [20–22]), ρ_{NL} is estimated from Eq. (9) to be about 4×10^{-6} m K/W which in principle is experimentally detectable [35]. The ISH voltage in Fig. 1(d) is estimated from Eq. (10) as $V_{ISH} \sim 0.06 \mu\text{V/K}$ (SM [39]) by using the typical parameters [35] $\theta_{SH} = 0.0037$, $\rho = 0.91 \mu\Omega\text{m}$ in Pt. Above T_C , the detection signal should decrease drastically due to the enhanced magnetic disorder [42].

Permitted by symmetry in hexagonal structure, there may exist the Dzyaloshinskii-Moriya interaction (DMI) [7, 25, 50], $H_{\text{DM}} = [D/(3\sqrt{3})] \sum_{\langle\langle i,j \rangle\rangle} \nu_{ij} \hat{z} \cdot (S_i \times S_j)$ with $\nu_{ij} = +1$ (-1) if the exchange between two next-nearest spins is clockwise (anticlockwise). DMI can induce magnon Hall effect [25] by breaking \mathcal{T} but does not generate topological difference between two valleys. To clarify the influence of DMI, we calculate κ_{xy}^v as a function of U in Fig. 3(a) for $D = 0, 0.05, 0.1$ meV. As expected, κ_{xy}^v becomes weaker under the effect of DMI, and can be enhanced by increasing U . Near the circled points $D = U$, the gap closing and reopening near one valley occur (SM [39]), and κ_{xy} changes drastically due to the sign change of Berry curvature.

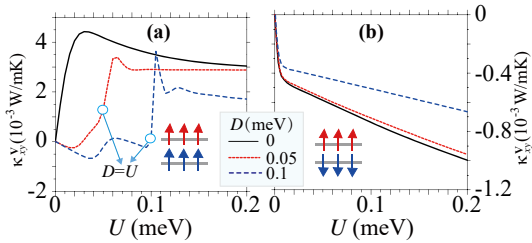


FIG. 3: Valley Hall conductivity as a function of potential U under the influence of DMI in (a) FM and (b) LAF samples at $T = 28$ K. The other parameters from CrBr_3 in Fig. 1 are taken. Pure valley current $\kappa_{xy}^K = -\kappa_{xy}^{K'}$ [39] is only present for $D = 0$ in both (a) and (b).

Moreover, we consider the influence of layered antiferromagnetic (LAF) order [31], which means each layer is FM while the FM orientation is opposite between two layers. For the LAF system, H_U in Eq. (1) should be replaced by $H_U = U \sum_i S_i^z$ (in the ground state, S_i^z is opposite for two layers). The results shown in Fig. 3(b) indicate that the layer polarity term H_U is still useful to strengthen the signal of κ_{xy}^v , reaching 1 mW/m K at $T = 28$ K for a weaker DMI. Compared with the FM bilayer case, the almost opposite Berry curvature [25, 39] of magnon bands for the LAF case hinders the enhancement of topological valley current. To induce H_U , the perpendicular magnetic field [29] is feasible besides doping. As U increases, a transition of LAF to FM [29] should happen, and a stronger topological valley signal is detectable.

Discussion—The picture of topological valley transport of magnons discussed in bilayer CrBr_3 also applies to multilayer FM CrBr_3 [32–34], bilayer or multilayer $\text{CrBr}_x\text{I}_{3-x}$ [46] or CrI_3 [30]. A particular issue is the Gilbert damping [17], for which the damping constant in Landau-Lifshitz-Gilbert equation is estimated as $\sim 10^{-4}$ [48–51] under the effects of the weak Rashba-type DMI or disorder. This damping should play negligible role in magnon valley transport due to topological protection [52], and is expected to change little in weak doping case $U \ll J$ we focus (the system can preserve insulating properties by adjusting gates). It is still an open question that whether more complicated mechanisms work for larger U . Additionally, it is promising in view of application if the physics discussed here is applied to other 2D FM insulators with higher Curie temperature.

This work shows that THz magnons are a new attractive platform for valleytronics beyond fermions and form the basis for valley-controlled magnonic applications. Our results will motivate the experimental exploration of valley-related magnon physics in 2D van der Waals magnets. Richer valley properties of topology and transport can be expected under the combined effect of magnetic order, symmetry breaking, and magnetic interactions.

We thank T. Yu and G. E. W. Bauer for helpful discussions. The work was supported by NSFC 61874057 and 11504179, the QingLan Project of Jiangsu Province (2019), 1311 Talent Program “DingXin Scholar” of NJUPT (2018) and Jiangsu Government Scholarship for Overseas Studies.

- [1] C. Gong, L. Li, Z. Li *et. al.*, *Nature* **546**, 265 (2017).
- [2] B. Huang, G. Clark, E. Navarro-Moratalla *et. al.*, *Nature* **546**, 270 (2017).
- [3] K. S. Burch, D. Mandrus, and J.-G. Park, *Nature* **563**, 47 (2018).
- [4] C. Gong and X. Zhang, *Science*, **363**, 706 (2019).
- [5] M. Gibertini, M. Koperski, A. F. Morpurgo, and K. S. Novoselov, *Nat. Nanotechnol.* **14**, 408 (2019).
- [6] S. S. Pershoguba, S. Banerjee, J. C. Lashley, J. Park, H. Ågren, G. Aeppli, and A. V. Balatsky, *Phys. Rev. X* **8**, 011010 (2018).
- [7] L. Chen, J.-H. Chung, B. Gao *et. al.*, *Phys. Rev. X* **8**, 041028 (2018).
- [8] A. Rycerz, J. Tworzydło, and C. W. J. Beenakker, *Nat. Phys.* **3**, 172 (2007).
- [9] K. F. Mak, K. L. McGill, J. Park, and P. L. McEuen, *Science* **344**, 1489 (2014).
- [10] X. Xu, W. Yao, D. Xiao, and T. F. Heinz, *Nat. Phys.* **10**, 343 (2014).
- [11] H. Pan, Z. Li, C.-C. Liu, G. Zhu, Z. Qiao, and Y. Yao, *Phys. Rev. Lett.* **112**, 106802 (2014).
- [12] Z. Niu, *New J. Phys.* **21**, 093044 (2019).
- [13] J. R. Shaibely, H. Yu, G. Clark *et. al.*, *Nat. Rev. Mater.* **1**, 16055 (2016).
- [14] S. A. Vitale, D. Nezich, J. O. Varghese *et. al.*, *Small* **14**, 1801483 (2018).
- [15] J. Noh, S. Huang, K. P. Chen, and M. C. Rechtsman, *Phys. Rev. Lett.* **120**, 063902 (2018).
- [16] J. Lu, C. Qiu, W. Deng, X. Huang, F. Li, F. Zhang, S. Chen, and Z. Liu, *Phys. Rev. Lett.* **120**, 116802 (2018).
- [17] A. V. Chumak, V. I. Vasyuchka, A. A. Serga, and B. Hillebrands, *Nat. Phys.* **11**, 453 (2015).
- [18] W. Jin, H. H. Kim, Z. Ye *et. al.*, *Nat. Commun.* **9**, 5122 (2018).
- [19] D. Xiao, W. Yao, and Q. Niu, *Phys. Rev. Lett.* **99**, 236809 (2007).
- [20] Y. Shimazaki, M. Yamamoto, I. V. Borzenets, K. Watanabe, T. Taniguchi, and S. Tarucha, *Nat. Phys.* **11**, 1032 (2015).
- [21] M. Sui, G. Chen, L. Ma *et. al.*, *Nat. Phys.* **11**, 1027 (2015).
- [22] R. V. Gorbachev, J. C. W. Song, G. L. Yu *et. al.*, *Science* **346**, 448 (2014).
- [23] V. A. Zyuzin and A. A. Kovalev, *Phys. Rev. Lett.* **117**, 217203 (2016).
- [24] R. Cheng, S. Okamoto, and D. Xiao, *Phys. Rev. Lett.* **117**, 217202 (2016).
- [25] S. A. Owerre, *Phys. Rev. B* **94**, 094405 (2016).
- [26] D. Xiao, M.-C. Chang, and Q. Niu, *Rev. Mod. Phys.* **82**, 1959 (2010).
- [27] Z. Wu, B. T. Zhou, X. Cai *et. al.*, *Nat. Commun.* **10**, 611 (2019).
- [28] J. Lee, K. F. Mak, and J. Shan, *Nat. Nanotechnol.* **11**, 421 (2016).
- [29] S. Jiang, J. Shan, and K. F. Mak, *Nat. Mater.* **17**, 406 (2018).
- [30] S. Jiang, L. Li, Z. Wang, K. F. Mak, and J. Shan, *Nat. Nanotechnol.* **13**, 549 (2018).
- [31] W. Chen, Z. Sun, Z. Wang, L. Gu, X. Xu, S. Wu, and C. Gao, *Science* **366**, 983 (2019).
- [32] Z. Zhang, J. Shang, C. Jiang, A. Rasmitha, W. Gao, and T. Yu, *Nano Lett.* **19**, 3138 (2019).
- [33] M. A. McGuire, *Crystals* **7**, 121 (2017).
- [34] N. Richter, D. Weber, F. Martin *et. al.*, *Phys. Rev. Mater.* **2**, 024004 (2018).
- [35] K. Uchida, J. Xiao, H. Adachi *et. al.*, *Nat. Mater.* **9**, 894 (2010).
- [36] G. E. W. Bauer, E. Saitoh, and B. J. van Wees, *Nat. mater.* **11**, 391 (2012).

- [37] L. J. Cornelissen, K. J. H. Peters, G. E. W. Bauer, R. A. Duine, and B. J. van Wees, Phys. Rev. B **94**, 014412 (2016).
- [38] E. McCann, Phys. Rev. B **74**, 161403(R) (2006).
- [39] See Supplemental Material for details on deriving Eqs. (5) and (9), observing transport signals in Figs. 1-3, estimating from Eq. (10) and discussing edge states.
- [40] H. Katsura, N. Nagaosa, and P. A. Lee, Phys. Rev. Lett. **104**, 066403 (2010).
- [41] J. H. Han and H. Lee, J. Phys. Soc. Jap. **86**, 011007 (2017).
- [42] Y. Onose, T. Ideue, H. Katsura, Y. Shiomi, N. Nagaosa, and Y. Tokura, Science **329**, 297 (2010).
- [43] D. A. Abanin, A. V. Shytov, L. S. Levitov, and B. I. Halperin, Phys. Rev. B **79**, 035304 (2009).
- [44] L. Webster, J.-A. Yan, Phys. Rev. B **98**, 144411 (2018).
- [45] H. Wang, V. Eyert, and U. Schwingenschlögl, J. Phys.: Condens. Matter **23**, 116003 (2011).
- [46] M. Abramchuk, S. Jaszewski, K. R. Metz *et. al.*, Adv. Mater. **30**, 1801325 (2018).
- [47] C. H. Ahn *et. al.*, Rev. Mod. Phys. **78**, 1185 (2006).
- [48] X. S. Wang and X. R. Wang, J. Phys. D: Appl. Phys. **51**, 194001 (2018).
- [49] W. Xing, L. Qiu, X. Wang *et. al.*, Phys. Rev. X **9**, 011026 (2019).
- [50] S. K. Kim, H. Ochoa, R. Zarzuela, and Y. Tserkovnyak, Phys. Rev. Lett. **117**, 227201 (2016).
- [51] A. A. Pervishko, M. I. Baglai, O. Eriksson, and D. Yudin, Sci. Rep. **8**, 17148 (2018).
- [52] A. Rückriegel, A. Brataas, and R. A. Duine, Phys. Rev. B **97**, 081106(R) (2018).